Non-monotonic variation of the exchange energy in double elliptic quantum dots

Non-monotonic variation of the exchange energy in double elliptic quantum dots

L-X Zhang, D V Melnikov and J-P Leburton

Beckman Institute for Advanced Science and Technology, University of Illinois at
Urbana-Champaign, Urbana, IL 61801, USA
and
Department of Electrical and Computer Engineering, University of Illinois at
Urbana-Champaign, Urbana, IL 61801, USA

E-mail: jleburto@illinois.edu

Abstract
We study the properties of a few-electron system confined in coupled elongated quantum dots
(QDs) using a model Gaussian potential and the numerical exact diagonalization technique. In
the absence of magnetic fields, as the aspect ratio r between the QD extensions in the directions
perpendicular and parallel to the coupling directions increases, the exchange energy exhibits a
sharp variation at the specific value $r = 3.9$, before (after) which the exchange energy increases
(declines). The sharp variation occurs because of a sudden change in the single-particle
configuration of the triplet state. The stability region with one electron in each of the QDs is
found to shrink, and finally vanishes as it becomes progressively easier to localize both
electrons into the QD with the lower electron potential energy. For $r > 3.9$, the first
singlet–triplet transition shifts to a small magnetic field.

(Some figures in this article are in colour only in the electronic version)

1. Introduction

Coupled quantum dots (QDs) based on two-dimensional electron gas (2DEG) formed with GaAs/AlGaAs heterostructures are promising candidates for quantum logic applications because of the ability to coherently manipulate the many-body spin states by using external electromagnetic fields [1–3]. Recently, a coherent controlled cycle of many-body state preparation, spin interaction and projective read-out has been achieved in laterally coupled QDs [4]. In such an experiment, the electromagnetic control of the exchange energy J, which drives the Rabi oscillations between the lowest singlet and triplet states, is of utmost importance. It is well known that the hyperfine interaction between the electron and nuclear spins competes with the exchange energy to destroy the singlet–triplet coherence [5]. Therefore, in order to retain the spin-state coherence in coupled GaAs/AlGaAs QDs, it is important to optimize the exchange energy to exceed the hyperfine interaction significantly.

A wealth of theoretical work has been devoted to study the exchange energy in coupled QD systems [6–13]. The main focus of these studies is the tunability of the exchange energy

by the electromagnetic fields and/or the parameters defining the interdot coupling strength, e.g. interdot separation and barrier height. The optimization of the exchange coupling J—given a fixed interdot distance, which is predetermined by the lithography of the top gates—has been rarely discussed. In this work, we investigate such a possibility by considering QDs elongated perpendicularly to the coupling direction. In this configuration, one can expect the overlap between the electron wavefunctions in the two QDs to increase, which will enhance their interactions. Our work is mainly motivated by this thought and also encouraged by the recent proposal of using coupled elongated QDs to construct robust spin-qubits with all-electrical qubit manipulation capabilities [14].

In this paper, we perform a detailed analysis of the two-electron system in coupled elongated QDs to show that the exchange coupling indeed becomes larger with increasing aspect ratio between the extensions of each QD perpendicular and parallel to the coupling direction ($r = R_y/R_x$). Our analysis based on the numerical exact diagonalization technique indicates that the cause of this enhancement is far from intuitive, while there is an optimum r value beyond which the exchange energy J decreases. Furthermore, for $r \geqslant 5$, we

1

find that the stability region for one electron in each QD shrinks to vanishing. Finally, the magnetic field, which defines the boundary between different spin phases of the system ground state, decreases with increasing r.

2. Model and method

The Hamiltonian for the coupled QD system is given by

$$H = H_{\text{orb}} + H_Z, \tag{1}$$

$$H_{\text{orb}} = h(\mathbf{r}_1) + h(\mathbf{r}_2) + C(\mathbf{r}_1, \mathbf{r}_2), \tag{2}$$

$$h(\mathbf{r}) = \frac{1}{2m^*}\left(\mathbf{p} + \frac{e}{c}\mathbf{A}\right)^2 + V(\mathbf{r}), \tag{3}$$

$$C(\mathbf{r}_1, \mathbf{r}_2) = e^2/\epsilon|\mathbf{r}_1 - \mathbf{r}_2|, \tag{4}$$

$$H_Z = g\mu_{\text{B}}\sum_i \mathbf{B} \cdot \mathbf{S}_i. \tag{5}$$

Here, we use the material parameters of GaAs, electron effective mass $m^* = 0.067m_e$, dielectric constant $\epsilon = 12.9$ and g-factor $g = -0.44$. μ_{B} is the Bohr magneton and $\mathbf{A} = \frac{1}{2}[-By, Bx, 0]$ is the vector potential for the constant magnetic field B oriented perpendicular to the QD plane (xy plane). The Zeeman effect simply induces a lowering of the single-particle (SP) and triplet energies by 13 and 25 μeV T^{-1}, respectively.

We use the following model potential for the coupled QD system [15]:

$$V(\mathbf{r}) = -V_{\text{L}}\text{e}^{-(x+d/2)^2/R_x^2 + y^2/R_y^2} - V_{\text{R}}\text{e}^{-(x-d/2)^2/R_x^2 + y^2/R_y^2}, \tag{6}$$

where V_{L} and V_{R} are the depth of the left and right QDs (equivalent to the QD gate voltages in experimental structures [1]) which can be independently varied, d is the interdot separation, and R_x and R_y are the radius of each QD in the x and y directions, respectively. In this work, we fix $R_x = 30$ nm and define the QD *aspect ratio* $r = R_y/R_x$. A numerical exact diagonalization technique is used to solve for the single- and two-electron energies. Details of the method are published elsewhere [15, 16].

Upon completion of the diagonalization procedure, we extract the SP energies e_i and the two-particle energies $E_i^{\text{S/T}}$. Here, 'S' ('T') denotes the singlet (triplet) state (in this paper, if not otherwise mentioned, 'singlet' and 'triplet' refer to the singlet and triplet states lowest in energy, respectively). The chemical potential of the Nth electron is given by the following equation [1]:
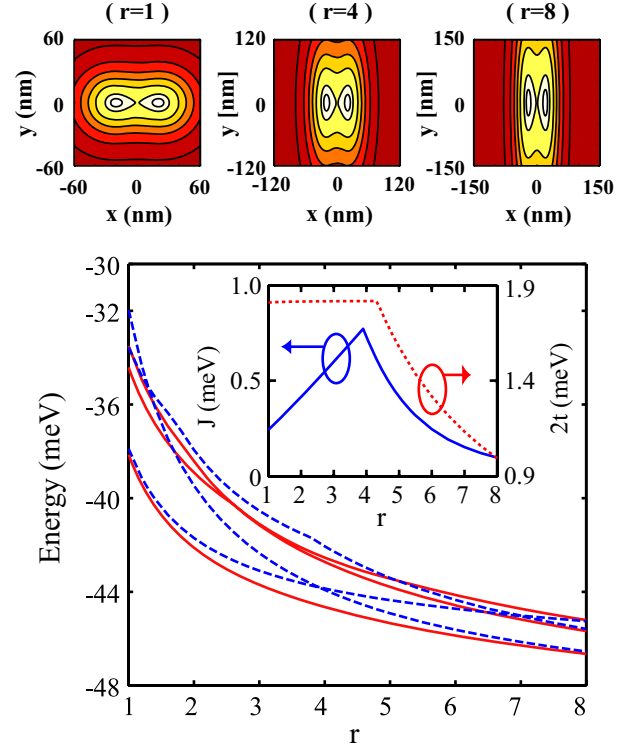
$$\mu(N) = E_0(N) - E_0(N-1), \tag{7}$$

where $E_0(N)$ (note that $E_0(0) = 0$) refers to the ground state energy with N electrons in the system. The exchange energy is given by

$$J = E_0^{\text{T}}(2) - E_0^{\text{S}}(2). \tag{8}$$

For further analysis, the total energy of the two-electron system is partitioned into the expectation values of the SP energy K and Coulomb energy C:

$$E^{\text{S/T}} = \langle\Psi_0^{\text{S/T}}|H|\Psi_0^{\text{S/T}}\rangle = \langle\Psi_0^{\text{S/T}}|h(\mathbf{r}_1) + h(\mathbf{r}_2)|\Psi_0^{\text{S/T}}\rangle$$
$$+ \langle\Psi_0^{\text{S/T}}|C(\mathbf{r}_1, \mathbf{r}_2)|\Psi_0^{\text{S/T}}\rangle = K^{\text{S/T}} + C^{\text{S/T}}, \tag{9}$$

Figure 1. Top panels: potential contour plots of coupled QD with $r = 1$ (left), $r = 4$ (middle) and $r = 8$ (right). Redder (darker gray) regions correspond to higher potential. Bottom panel: three lowest singlet (red/gray, solid lines) and triplet (blue/dark gray, dashed lines) energy levels as a function of QD aspect ratio r. The inset shows r dependence of the exchange energy J (blue/dark gray, solid) and tunnel coupling $2t$ (red/gray, dotted). For all panels, $V_{\text{L}} = V_{\text{R}} = 25$ meV, $d = 50$ nm, $B = 0$ T.

while the spectral function is defined as the projection coefficients of the lowest singlet and triplet states onto the SP product states [17]:

$$\alpha_{k,l}^{\text{S/T}} = \langle\psi_k(\mathbf{r}_1)\psi_l(\mathbf{r}_2)|\Psi_0^{\text{S/T}}(\mathbf{r}_1, \mathbf{r}_2)\rangle. \tag{10}$$

The electron density is given by

$$\rho^{\text{S/T}}(\mathbf{r}_1) = \int |\Psi_0^{\text{S/T}}(\mathbf{r}_1, \mathbf{r}_2)|^2 \, \text{d}\mathbf{r}_2. \tag{11}$$

Finally, the expectation value of the parity operator is given by

$$\langle\hat{P}^{\text{S/T}}\rangle = \langle\Psi_0^{\text{S/T}}(x_1, y_1, x_2, y_2)|\Psi_0^{\text{S/T}}(-x_1, -y_1, -x_2, -y_2)\rangle, \tag{12}$$
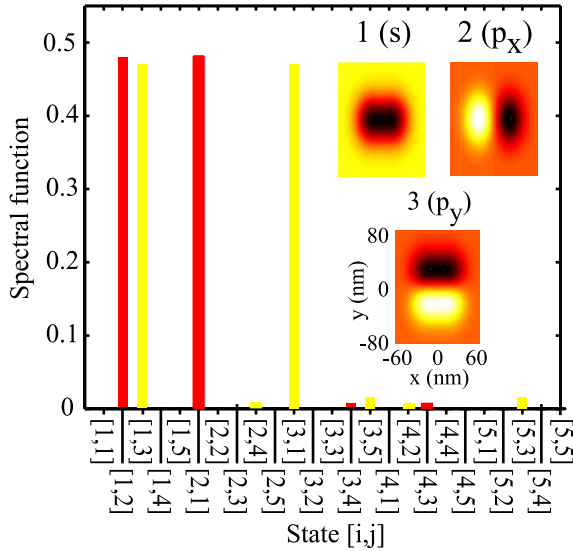
and for the parity operator along the y axis

$$\langle\hat{P}_y^{\text{S/T}}\rangle = \langle\Psi_0^{\text{S/T}}(x_1, y_1, x_2, y_2)|\Psi_0^{\text{S/T}}(x_1, -y_1, x_2, -y_2)\rangle. \tag{13}$$

3. Results

3.1. Aspect ratio dependence of the exchange energy

Figure 1 top panels show the potential contour plots $r = 1$ (left), $r = 4$ (middle) and $r = 8$ (right). As r increases, the potential becomes more elongated in the y direction, while the

Figure 2. Spectral decomposition of the two-electron wavefunction onto different single-particle pairs. The red (dark) columns are for $r = 3.9$, while the yellow (bright) columns are for $r = 4$. The inset shows the contour plots of the lowest three single-particle states in ascending order (indicated by numbers) of energy for both $r = 3.9$ and 4. The state symmetry is shown in parentheses.

effective interdot distance (i.e. the x distance between the two minima of the potential) and the interdot barrier height remain constant at 40 nm and 1.98 meV, respectively.

In the lower panel of figure 1, we plot the three lowest singlet (red/gray, solid) and triplet (blue/dark gray, dashed) energy levels as a function of r. With increasing r, the SP energies decrease (not shown), resulting in the decrease of the two-particle energy levels. We note that the lowest energy of the singlet state ($E_0^S(2)$) decreases smoothly with r, while the lowest energy of the triplet state ($E_0^T(2)$) exhibits a cusp at $r = 3.9$ because of the crossing of the lowest two triplet state energy levels. This cusp results in a sharp variation in the exchange energy dependence on r, which is shown in the inset of the lower panel of figure 1. In the same inset, we show the variation of the tunnel coupling $2t = e_1 - e_0$. For $r \leqslant 4.3$, the SP ground and first excited states have s and p_x characters, respectively, and $2t$ barely increases from 1.8105 to 1.8114 meV with increasing r, because the energy contributions from the y direction to e_0 and e_1 cancel out. For $r > 4.3$, the SP first excited state bears a p_y character, which causes $2t$ to decrease monotonically with r.

In order to investigate in detail the cusp in the lowest triplet state energy, or the crossing between the two lowest triplet levels in the lower panel of figure 1, we plot in figure 2 the spectral function of the two-electron wavefunction. It is seen that at $r = 3.9$ the triplet mainly consists of the [1, 2] and [2, 1] SP state pair, while at $r = 4$ it mainly consists of the [1, 3] and [3, 1] SP state pair. Here, 1, 2 and 3 denote the SP states in ascending energy, which have s, p_x and p_y characters, respectively, as shown in figure 2 inset. Since the energy ordering of these SP states does not change as r changes from 3.9 to 4 (not shown here), the cusp in the lowest triplet state is due to a sudden transition of the triplet wavefunction from occupying an sp_x pair to an sp_y pair.
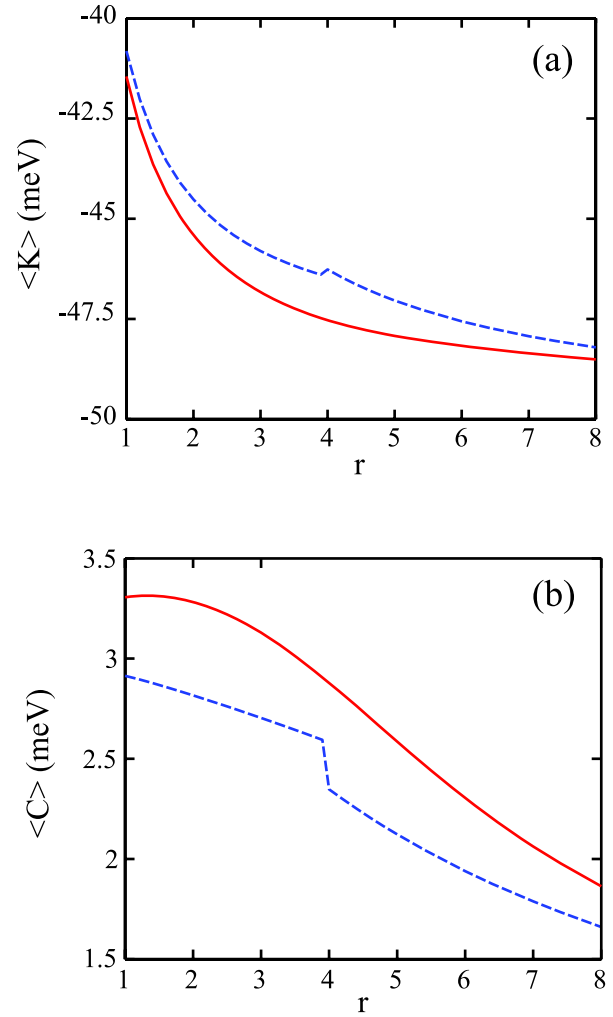
Figure 3. (a) Single-particle energy contribution $\langle K \rangle$ as a function of QD aspect ratio r. The red/gray, solid (blue/dark gray, dashed) line is for the singlet (triplet) state. (b) Coulomb energy contribution $\langle C \rangle$ as a function of QD aspect ratio r. The red/gray, solid (blue/dark gray, dashed) line is for the singlet (triplet) state.

In figure 3, we plot separately the (a) SP $\langle K \rangle$ and (b) Coulomb $\langle C \rangle$ contributions to the singlet and triplet state energies as a function of the QD aspect ratio r. As r increases, the general trend for all these energy terms is to decrease, leading to decreasing singlet and triplet energies shown in figure 1. For the singlet state, both $\langle K \rangle$ and $\langle C \rangle$ terms decrease smoothly with r. For the triplet state, however, a discontinuity is seen from $r = 3.9$ to 4: $\langle K \rangle$ ($\langle C \rangle$) suddenly increases (decreases) by 0.128 (0.607) meV. It now becomes clear that the transition of the SP configuration shown in figure 2 from the sp_x pair to the sp_y pair is favored by the lowering of the Coulomb interaction despite the increase in the SP energy.

As a consequence of the sudden change in the SP occupation, the y symmetry P_y of the two-electron wavefunction of the lowest triplet state changes abruptly from 1 to -1, which is validated by direct calculation of P_y. We point out that the crossing between the lowest two triplet states by increasing r is allowed because they possess opposite y symmetry, which exemplifies the general von Neumann–Wigner

theorem relating the molecular energy levels to the two-electron wavefunction symmetry [18, 19].

The contour plots in figure 4 clearly show that, from $r = 3.9$ (first row) to 4 (second row), the electron density in the lowest singlet state barely changes, while the density in the lowest triplet state changes abruptly from two peaks localized in the left and right QDs (the separation of two peaks in the x direction is $\sim$40 nm) to four peaks separated along both x and y directions (separation between peaks in the x and y directions are 20 and 40 nm, respectively), again due to the sudden change in the SP configuration. The third row in figure 4 shows that at $r = 8$, both the singlet and triplet densities exhibit four peaks separated in both the x and y directions. Our analysis shows that, from $r = 4$ to 8, the left and right peaks in the singlet state density gradually separate into four peaks and the separation between the top two and bottom two peaks in the triplet state density smoothly increases. Such electron localization effects at large r are discussed for other many-electron QD systems with weak confinement, see, for example, [20] and references therein.

3.2. Stability diagrams

In figure 5, upper panels, we plot the stability diagrams [1] of the coupled QDs for $r = 1$ (left), $r = 3$ (middle) and $r = 5$ (right) for $R_x = 30$ nm, $d = 50$ nm and $B = 0$ T. The solid curves indicated by arrows show the computed contours, where chemical potentials of the first electron (red), the second electron in the singlet state (green) and second electron in the triplet state (blue) are equal to the reference value ($\mu(1) = \mu^S(2) = \mu^T(2) = -21$ meV). According to the general shape of the stability diagram for coupled QDs [1], we use dotted straight lines on the diagrams to separate different charge states indicated by discrete electron numbers on the left and right QDs, e.g. $(0, 1)$ means zero electrons on the left QD and one electron on the right QD. Specifically, the boundaries between the $(1, 1)$ and $(0, 2)$ (or $(2, 0)$) states are taken extending from the point on the $\mu^S(2)$ curve at which the curvature is the largest for $V_L \neq V_R$, e.g. point C on the upper left panel and parallel to the main diagonal. In the absence of a magnetic field ($B = 0$), the $\mu^S(2)$ curve is the boundary between one and two electrons in the system (in the linear transport regime wherein the source and drain chemical potentials are nearly the same). Based on this fact, we extrapolate from the first off-diagonal triple point (e.g. point C on the upper left panel) to get the boundary between two- and three-electron states (green dotted curve indicated by $\mu(3)$). Here, we assume that the triple point separation between charge states $(1, 0)$ and $(2, 1)$ (or between the $(0, 1)$ and $(1, 2)$) is the same as the separation between the $(0, 0)$ and $(1, 1)$ states[1].

In figure 5, the double–triple point (DTP) separation (i.e. the separation between the crossing points of $\mu(1)$ and $\mu(2)$ curves with $V_L = V_R$) is measured to decrease with r: for the singlet (triplet) state, the DTP separation measured in $\Delta V_L = \Delta V_R$ is 5.181 (5.269) meV, 4.128 (4.725) meV and 3.473

---

[1] We emphasize that the boundary between two- and three-electron states are *not* computed. In other words, the $\mu(3)$ curves on the diagrams are guides to the eyes to delimit the charge states for two electrons in the coupled QDs.
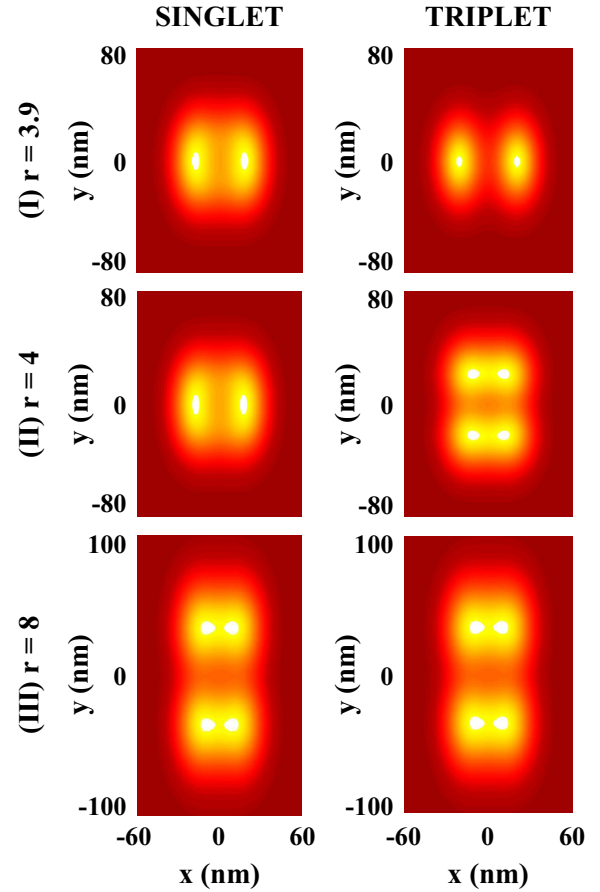

SINGLET   **TRIPLET**

Figure 4. Contour plots of the electron density for both singlet (left column) and triplet (right column). Rows I, II and III are for $r = 3.9$, $r = 4$ and $r = 8$, respectively. In the plots, redder (darker gray) regions correspond to lower electron density.

(3.907) meV for $r = 1$, 3 and 5, respectively. This decreasing trend of the DTP separation is readily seen by combining the effects of r on $2t$ and C shown in the inset of figures 1(b) and 3(b), respectively. Both quantities decrease with r, leading to a decreasing DTP separation, which is defined by the sum $2t + C$. The decreasing DTP separation suggests that coupling between the two QDs decreases with r [1]. We note that this refers to the coupling in either the singlet or the triplet state. However, the exchange coupling (energy) in this particular case exhibits a non-monotonic dependence on r (figure 1(b), inset).

One important feature shown in figure 5 is that, as r increases, the distance between the triple points on the main diagonal and the first off-diagonal (e.g. points B and C in the upper left panel of figure 5) becomes smaller and at large r these triple points coincide. Consequently, the $(1, 1)$ stability region shrinks and finally disappears. This is because, at large aspect ratios, even a small amount of interdot detuning can localize both electrons into the QD with the lower electron potential energy, resulting in an unstable $(1, 1)$ charge state. The boundary $\mu^T(2)$ at $r = 5$ suggests that the $(1, 1)$ charge state is also unstable for the triplet state, although the $\mu^S(2)$ and $\mu^T(2)$ curves evolve in different fashion as r increases.

After locating the different charge stable regions on the stability diagram, we now investigate the interdot detuning
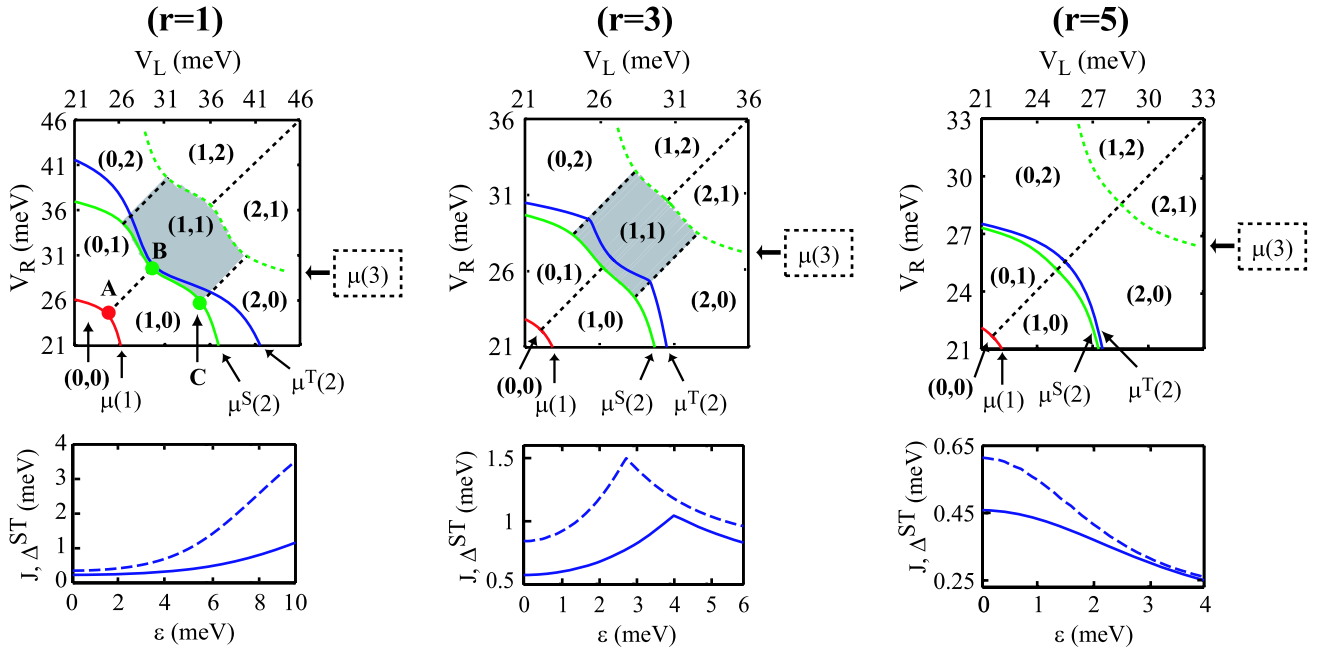
Figure 5. Top panels: stability diagrams for $r = 1$ (left), $r = 3$ (middle) and $r = 5$ (right). In each diagram, the red, green and blue curves (solid) are computed contour lines at which the chemical potential $\mu(1)$, $\mu^S(2)$ and $\mu^T(2)$ is equal to the reference value $\mu_{ref} = -21$ meV, respectively. Curves for different chemical potentials are also indicated by arrows. The dotted straight lines are a guide for eyes separating different stable charge states. Note that the exact locations of the $\mu(3)$ curve (green dotted curve) and (1, 2), (2, 1) regions are not computed. In the left two top panels, the (1, 1) region is indicated by the shaded area. In the leftmost upper panel, we also indicate the double-triple points A and B. Point C is where the $\mu^S(2)$ curve has the largest curvature for $V_L \neq V_R$. For corresponding QD aspect ratios, the bottom panels show J (solid curves) as a function of interdot detuning $\epsilon = V_L - V_R$ from the center of the (1, 1) region. The dashed curves on the bottom panels show the separation (Δ^{ST}) between the contour lines of $\mu^S(2)$ and $\mu^T(2)$ projected along the main diagonal as a function of interdot detuning $\epsilon = V_L - V_R$. All data are obtained at $R_x = 30$ nm, $d = 50$ nm and $B = 0$ T.

effect by departing from the center of the (1, 1) region along the direction perpendicular to the main diagonal, i.e. $V_L + V_R = $ constant. Such detuning effects are important as two electrons transfer to a single QD, which is a key step in spin coherent manipulation and spin-to-charge conversion in two-electron double QD experiments for quantum logic gate applications [2, 4].

The solid curves in figure 5, lower panels, show the exchange energy J as a function of interdot detuning $\epsilon = V_L - V_R$ along the $V_L + V_R = $ constant line ($\epsilon = 0$ is chosen at the (1, 1) region center). In the case of coupled circular QDs ($r = 1$), with increasing ϵ, both singlet and triplet states localize progressively into the QD with the lower electron potential energy, leading to a monotonic increase of J. Such a dependence is similar to recent experimental [4] and theoretical [21] results. For $r = 3$, a sharp cusp in J occurs at $\epsilon \sim 4$ meV before which J monotonically increases with ϵ. This cusp is induced by a sudden SP configuration change in the lowest triplet state, which is similar to the effects seen in figure 1 and analyzed in figure 2, albeit here the perturbation in the Hamiltonian is introduced by interdot detuning instead of deformation effects. More detailed analysis of the two-particle energies and electron density for the $r = 1$ and 3 cases can be found in [22][2]. For $r = 5$, we observe that

the exchange energy decreases monotonically with ϵ, because the Coulomb energy difference between the singlet and triplet states becomes smaller as the two electrons in both the singlet and triplet states localize at the opposite ends of the lower single QD to minimize their Coulomb interaction.

In the lower panels of figure 5, we also plot the ϵ dependence of Δ^{ST} (dashed curves), the difference between the $\mu^S(2)$ and $\mu^T(2)$ curves projected along the main diagonal. Δ^{ST} is relevant in this context because in coupled QD experiments the chemical potential contour lines are mapped out by single-electron charging measurements, which provides useful information on the electronic structure of the QD [1, 2, 23]. Here, we notice that, although the general detuning dependence is similar between J and Δ^{ST}, a linear factor is not sufficient to scale values of J to overlap with those of Δ^{ST} because the two quantities are extracted under different bias conditions. It should be pointed out that transport experiments measure the quantity Δ^{ST}, which differs quantitatively from the exchange energy J. In figure 6, we plot the charge stability diagram of the coupled QDs for $r = 1$ (left), $r = 3$ (middle) and $r = 5$ (right) for $R_x = 30$ nm, $d = 60$ nm and $B = 0$ T. Compared to the data in figure 5, which correspond to strongly coupled QDs, at $d = 60$ nm, the (1, 1) region does not vanish for $r = 5$ because, as the QDs are more decoupled, both the interdot distance and interdot barrier height become larger, which require a larger interdot detuning to 'push' both electrons into the QD with the lower electron potential energy.

---

[2] In this reference, the detuning is measured by fixing $V_R = $ constant, while in the text it is measured perpendicular to the main diagonal of the stability diagram, i.e. $V_L + V_R = $ constant.
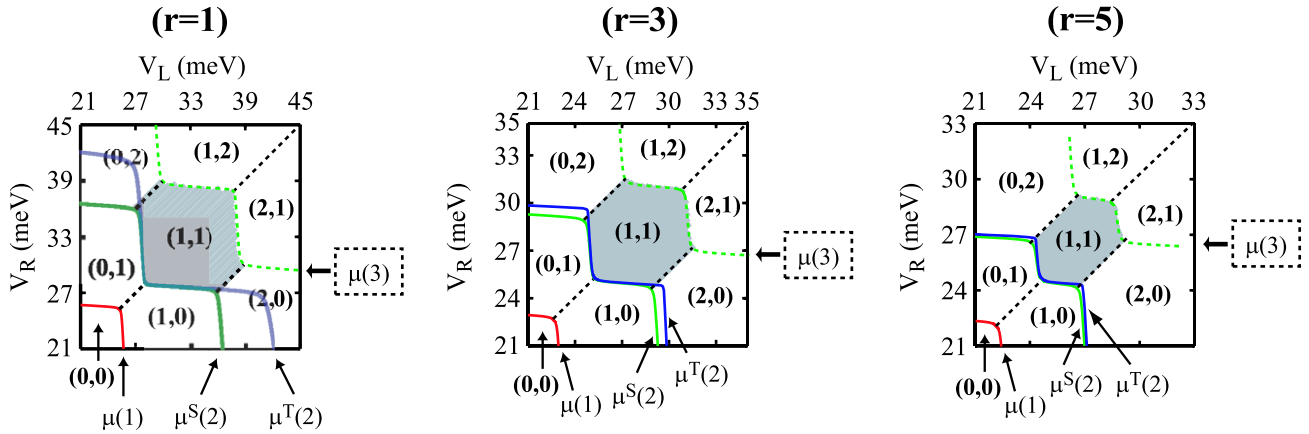
Figure 6. Stability diagrams for $r = 1$ (left), $r = 3$ (middle) and $r = 5$ (right). In each diagram, the red, green and blue curves (solid) are computed contour lines at which the chemical potential $\mu(1)$, $\mu^S(2)$ and $\mu^T(2)$ equal to the reference value $\mu_{ref} = -19$ meV, respectively. Curves for different chemical potentials are also indicated by arrows. The dotted straight lines are a guide for eyes separating different stable charge states. Note that the exact locations of the $\mu(3)$ curve (green dotted curve) and (1, 2), (2, 1) regions are not computed. In each panel, the (1, 1) region is indicated by the shaded area. All data are obtained at $R_x = 30$ nm, $d = 60$ nm and $B = 0$ T.

3.3. Spin phase diagram

In this section, we discuss the variation of the exchange energy J as a function of both r and B. By identifying the regions where J assumes different signs, we construct the spin phase diagram in which the two-electron ground state spin state (either $S = 0$ or 1) is shown as a function of r and B [24, 25].

In figure 7, we plot the exchange energy J as a function of the QD aspect ratio r and the magnetic field B perpendicular to the xy plane. At fixed r, as B increases, J decreases from its value at $B = 0$ T to become negative and saturate at very large magnetic field, as previously reported [6–12]. We note that, at intermediate r ($r \sim 4$), J changes much faster with B than at small or large r. This B-field effect at intermediate r values is associated with the 2D confinement of the QDs, i.e. near $r = 4$ the SP level separations in the x and y directions are comparable (cf figure 1, lower inset, $2t$ curve). We also note that, with increasing r, the relative change of J is small for $B \sim 1$ T, while it is much larger for $B \sim 0$ T or $B \sim 2$ T. The kink in J at $B = 0$ T (cf figure 1, lower inset, J curve), due to the crossing of two lowest triplet levels, does not exist for $B \neq 0$ T because a nonzero magnetic field couples the SP states with different Cartesian symmetries, thereby removing the condition for the crossing of the lowest two triplet states. In the investigated ranges of r and B, J assumes a maximum (minimum) value of 0.773 (-0.372) meV at $r \approx 3.9$, $B \approx 0$ T ($r \approx 4.4$, $B \approx 1.6$ T).

The projected contour plots in figure 7 show that the first singlet–triplet transition (at which J first crosses zero as B increases from zero at fixed r) occurs at a smaller B value as r increases, which is shown by the thick white dashed curve on the contour plot in figure 7. Such a dependence can be understood by observing that, in the absence of the B field, as r increases the SP energy spacing decreases and, for a larger r, a smaller magnetic field is needed to further decrease the SP spacing and bring the triplet state to the ground state with the aid of the Coulomb energy difference between the singlet and triplet states. At higher magnetic field and larger r, we observe
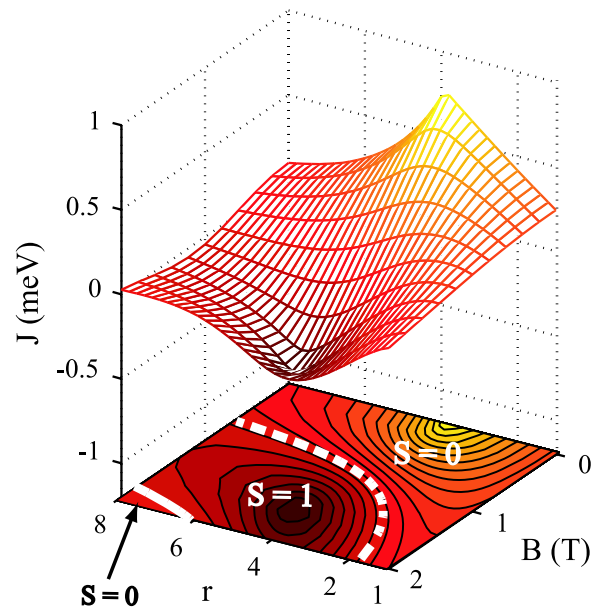
Figure 7. Mesh (contour) plot of the exchange energy J as a function of QD aspect ratio r and the magnetic field B. The thick white curves (solid and dashed) on the contour plot correspond to $J = 0$. Total spin of the two-electron ground state is given in different regions. Redder (darker gray) regions correspond to lower J value.

another contour line for $J = 0$ (thick solid white curve at the lower left corner). The reappearance of the singlet state as the ground state is reminiscent of the singlet–triplet oscillation found for a two-electron single QD and also reported elsewhere for two-electron QDs with strong confinement [24–26]. In the foregoing discussion, we had not included the Zeeman energy for the triplet state, which would lower the triplet energy such that the boundary for the first singlet–triplet transition (thick white dashed curve) would shift to lower values of r and B, while the second singlet–triplet transition (thick white solid curve) would move to higher values of r and B.

4. Conclusions

We have shown that the exchange energy between two electrons in coupled elongated quantum dots is enhanced by increasing the aspect ratio of the dots in the direction perpendicular to the coupling direction. However, there is an optimum aspect ratio beyond which the electron density in each dot starts to localize and the exchange energy decreases. With increasing aspect ratio, the (1, 1) region becomes unstable with respect to interdot detuning, which is undesirable for two spin-qubit operations. We have also shown that the exchange energy in symmetrically biased coupled quantum dots is tunable between maximum (positive) and minimum (negative) values by varying the magnetic field and the QD aspect ratio.

Acknowledgments

References

[1] van der Wiel W G, Franceschi S D, Elzerman J M, Fujisawa T, Tarucha S and Kouwenhouven L P 2003 *Rev. Mod. Phys.* **75** 1–22
[2] Hanson R, Kouwenhoven L P, Petta J R, Tarucha S and Vandersypen L M K 2007 *Rev. Mod. Phys.* **79** 1217–65
[3] Loss D and DiVincenzo D P 1998 *Phys. Rev.* A **57** 120–6
[4] Petta J R, Johnson A C, Taylor J M, Laird E A, Yacoby A, Lukin M D, Marcus C M, Hanson M P and Gossard A C 2005 *Science* **309** 2180–4
[5] Laird E A, Petta J R, Johnson A C, Marcus C M, Yacoby A, Hanson M P and Gossard A C 2006 *Phys. Rev. Lett.* **97** 056801
[6] Burkard G, Loss D and DiVincenzo D P 1999 *Phys. Rev.* B **59** 2070–8
[7] Dybalski W and Hawrylak P 2005 *Phys. Rev.* B **72** 205432
[8] Hu X and Das Sarma S 2000 *Phys. Rev.* A **61** 062301
[9] Szafran B, Peeters F M and Bednarek S 2004 *Phys. Rev.* B **70** 205318
[10] Bellucci D, Rontani M, Troiani F, Goldoni G and Molinari E 2004 *Phys. Rev.* B **69** 201308(R)
[11] Pedersen J, Flindt C, Mortensen N A and Jauho A-P 2007 *Phys. Rev.* B **76** 125323
[12] Harju A, Siljamäki S and Nieminen R M 2002 *Phys. Rev.* B **65** 075309
[13] Zhang L-X, Melnikov D V and Leburton J-P 2006 *Phys. Rev.* B **74** 205306
[14] Kyriakydis J and Burkard G 2007 *Phys. Rev.* B **75** 115324
[15] Zhang L-X, Melnikov D V and Leburton J-P 2007 *IEEE Trans. Nanotechnol.* **6** 250–5
[16] Melnikov D V and Leburton J-P 2006 *Phys. Rev.* B **73** 085320
[17] Melnikov D V and Leburton J-P 2006 *Phys. Rev.* B **73** 155301
[18] von Neumann J and Wigner E 1929 *Z. Phys.* **30** 465–70
[19] Landau L D and Lifshitz E 1977 *Quantum Mechanics: Non-Relativistic Theory* (Oxford: Pergamon)
[20] Bednarek S, Chwiej T, Adamowski J and Szafran B 2003 *Phys. Rev.* B **67** 205316
[21] Stopa M and Marcus C M 2008 *Nano Lett.* **8** 1778–82
[22] Zhang L-X, Melnikov D V and Leburton J-P 2008 *Phys. Rev.* B **78** 085310
[23] Johnson A C, Petta J R, Marcus C M, Hanson M P and Gossard A C 2005 *Phys. Rev.* B **72** 165308
[24] Harju A, Siljamäki S and Nieminen R M 2002 *Phys. Rev. Lett.* **88** 226804
[25] Helle M, Harju A and Nieminen R M 2005 *Phys. Rev.* B **72** 205329
[26] Wagner M, Merkt U and Chaplik A V 1992 *Phys. Rev.* B **45** 1951–4